SUPPLEMENTARY MATERIALS: Craton Formation by Underplating and Development of the MLD: Evidence from Bayesian Surface Wave Inversion

Alistair Boyce[1], Thomas Bodin[1], Stephanie Durand[1], Dorian Soergel[1,2], and Eric Debayle[1]

[1]Université Claude Bernard Lyon 1, ENS de Lyon, France
[2]Department of Earth and Planetary Science, University of California, Berkeley, USA

alistair.boyce@univ-lyon1.fr @alistair_boyce alistairboyce11.github.io

EGU24-2015 16/04/2024

Xi at 150km depth w.r.t. mean value in each model

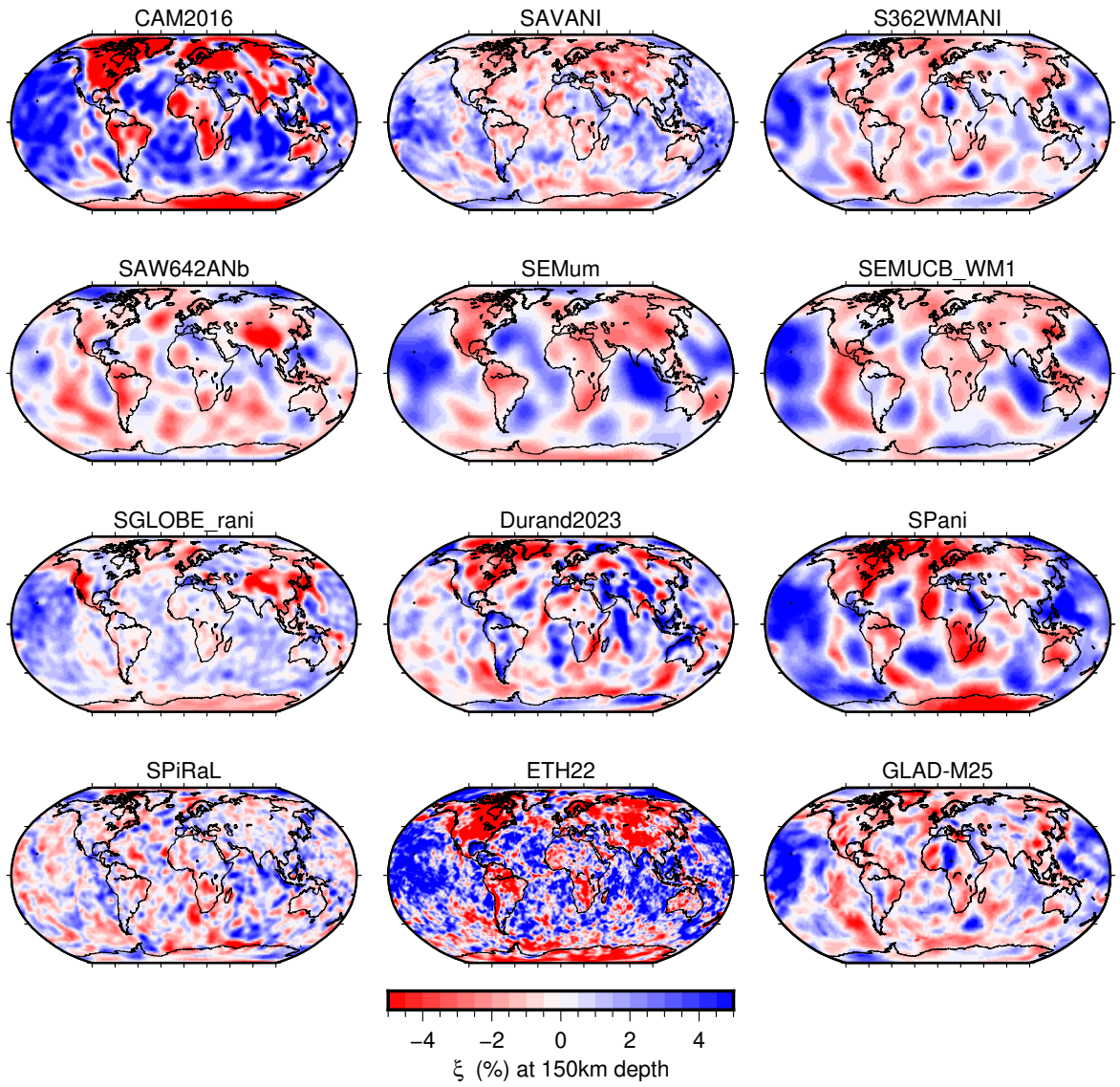

Twelve global radially anisotropic tomographic models plotted at 150 km depth with respect to the mean value in each model.

Boyce et al., (2024)

Xi at 150km depth w.r.t. PREM

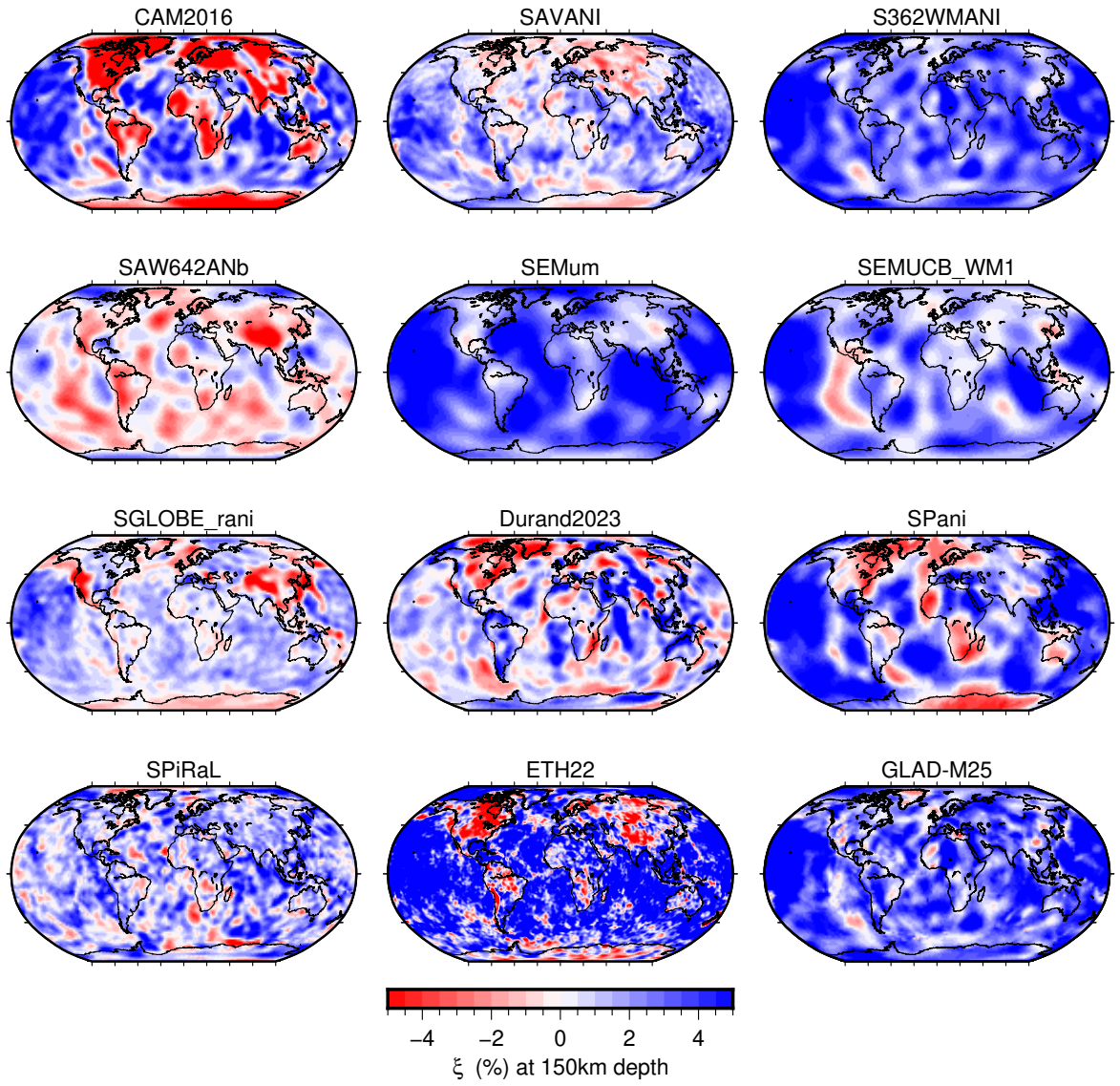

Twelve global radially anisotropic tomographic models plotted at 150 km depth with respect to anisotropic PREM model (Dziewonski & Anderson, 1981).

Boyce et al., (2024)

Xi at 150km depth (absolute value)

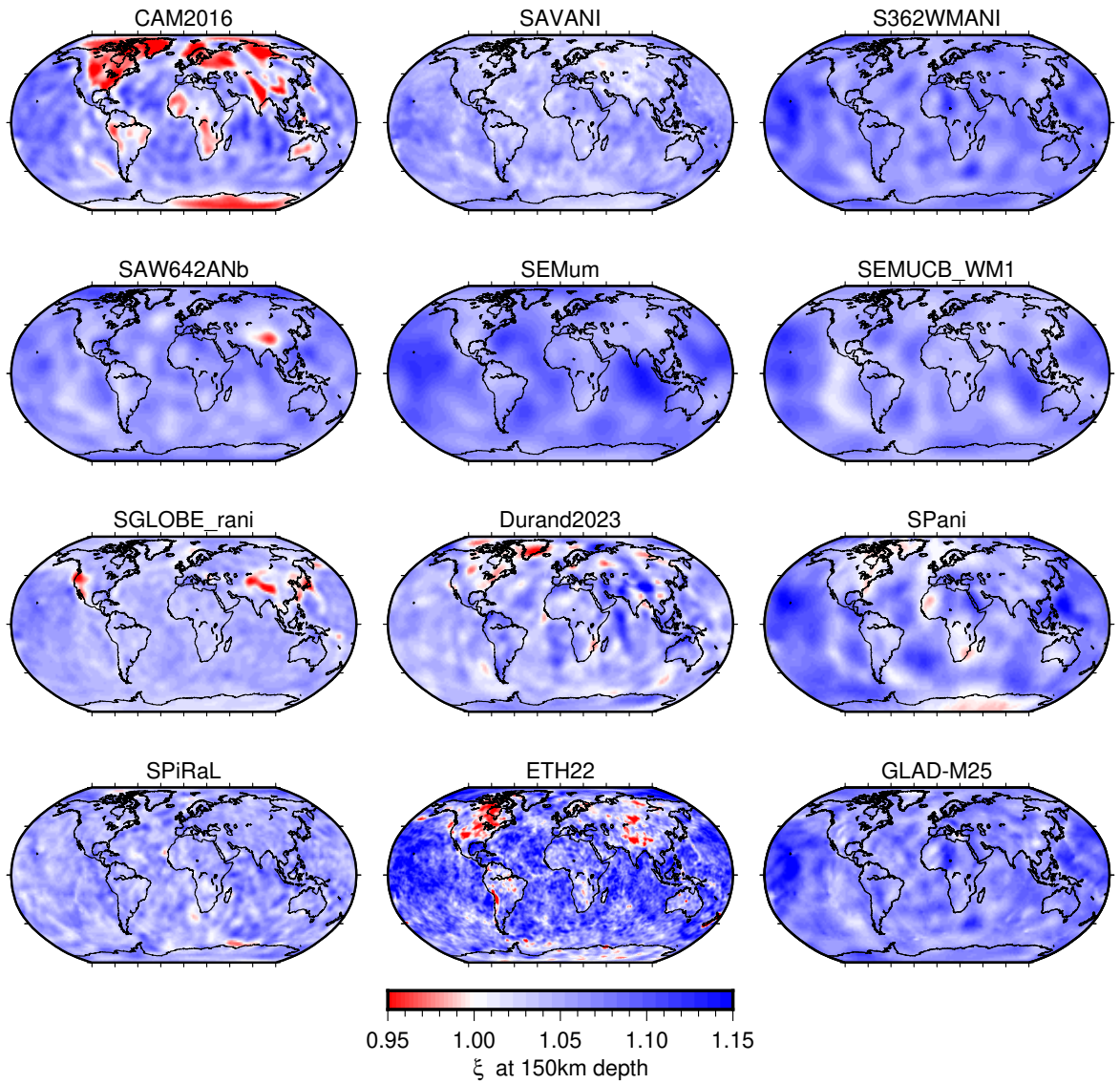

Twelve global radially anisotropic tomographic models plotted as the absolute value at 150 km depth. Note asymmetric color scale.

Boyce et al., (2024)

Vsv & Xi profiles from published tomographic models

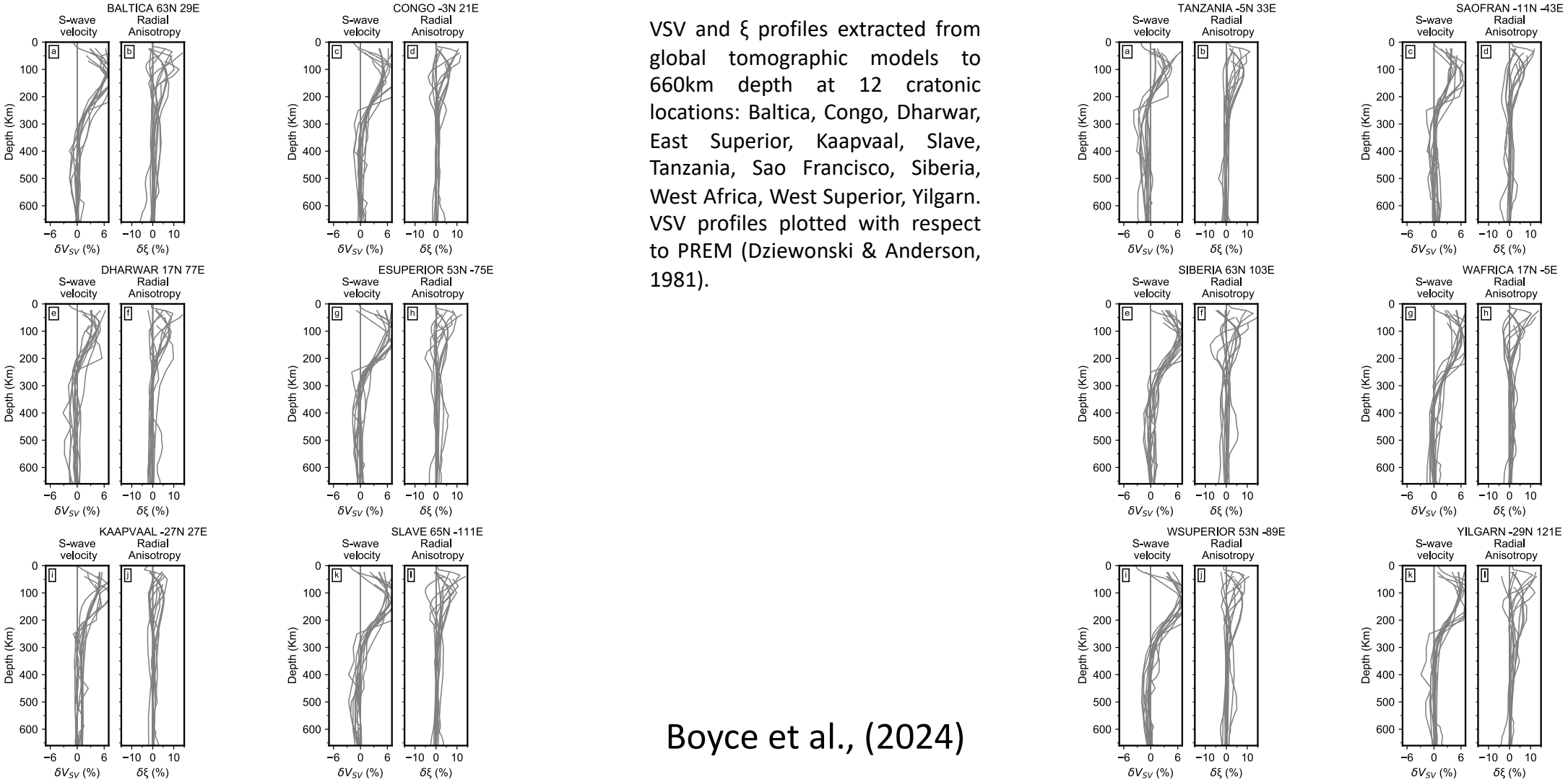

VSV and ξ profiles extracted from global tomographic models to 660km depth at 12 cratonic locations: Baltica, Congo, Dharwar, East Superior, Kaapvaal, Slave, Tanzania, Sao Francisco, Siberia, West Africa, West Superior, Yilgarn. VSV profiles plotted with respect to PREM (Dziewonski & Anderson, 1981).

Boyce et al., (2024)

Dispersion curve data sets

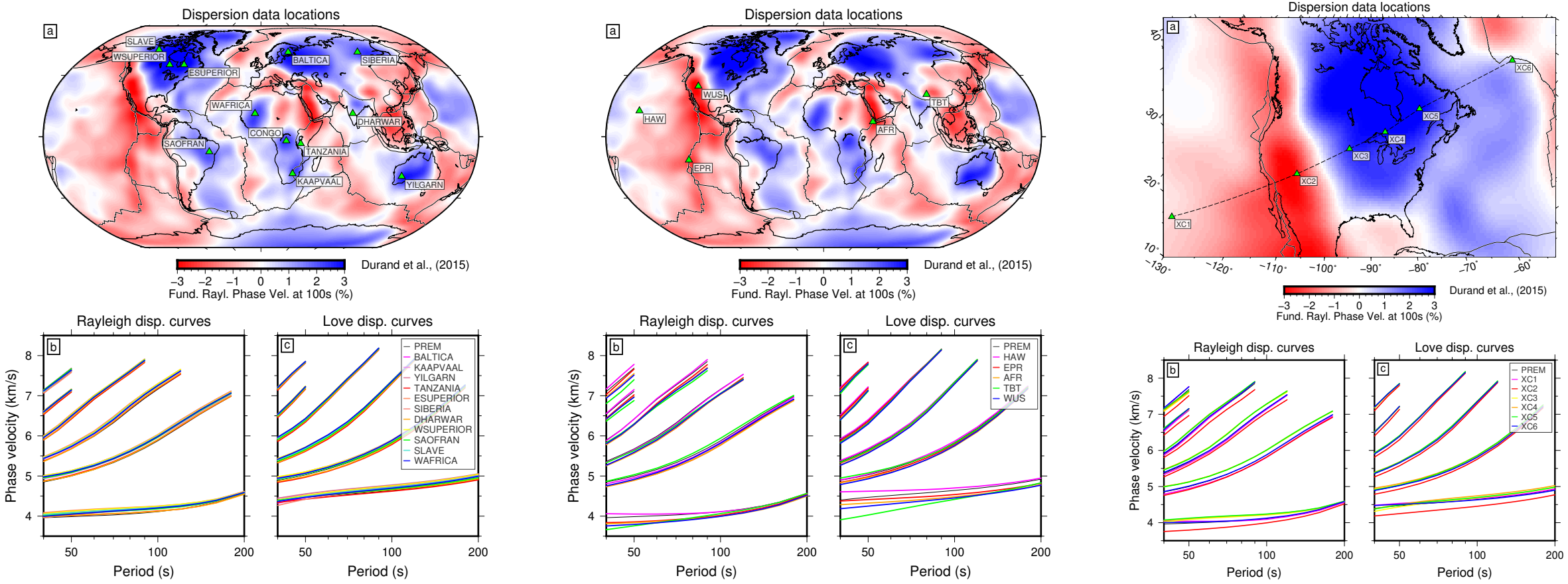

(a) Fundamental mode Rayleigh wave phase velocity map at 100 s period from Durand et al. (2015) with twelve cratonic locations (LEFT), five active tectonic locations (CENTER) and six cross-section points across North America (RIGHT) shown (green triangles). Rayleigh (b) and Love (c) fundamental and overtone (1–5) dispersion curves used in the inversions.

Boyce et al., (2024)

Sensitivity kernels

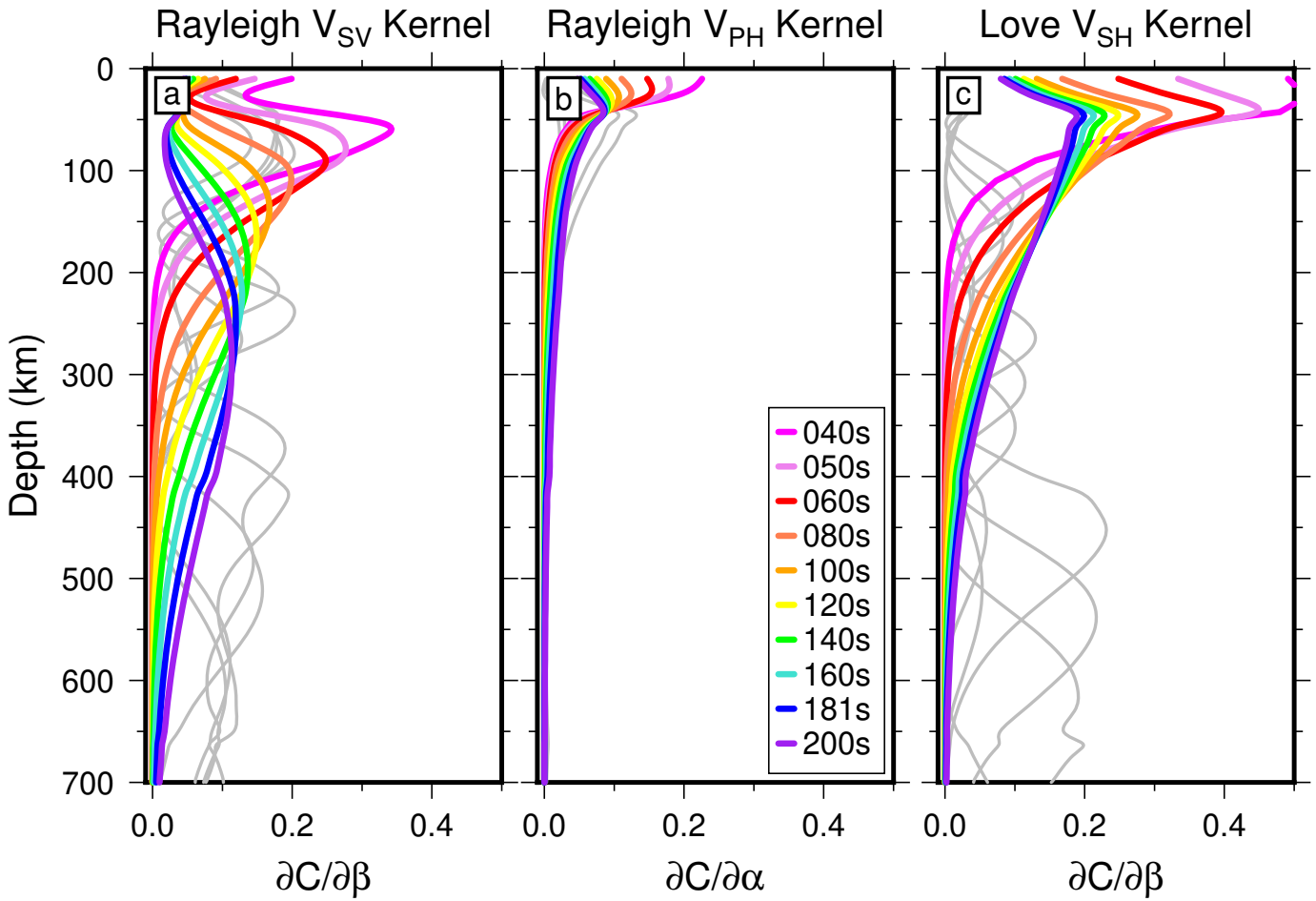

Fundamental mode (coloured) and 3rd overtone (gray) phase velocity (C) sensitivity kernels for Rayleigh (VSV and VPH, a,b) and Love (VSH, c) waves at a range of periods for the modified PREM reference model.

Boyce et al., (2024)

Bayesian synthetic tests

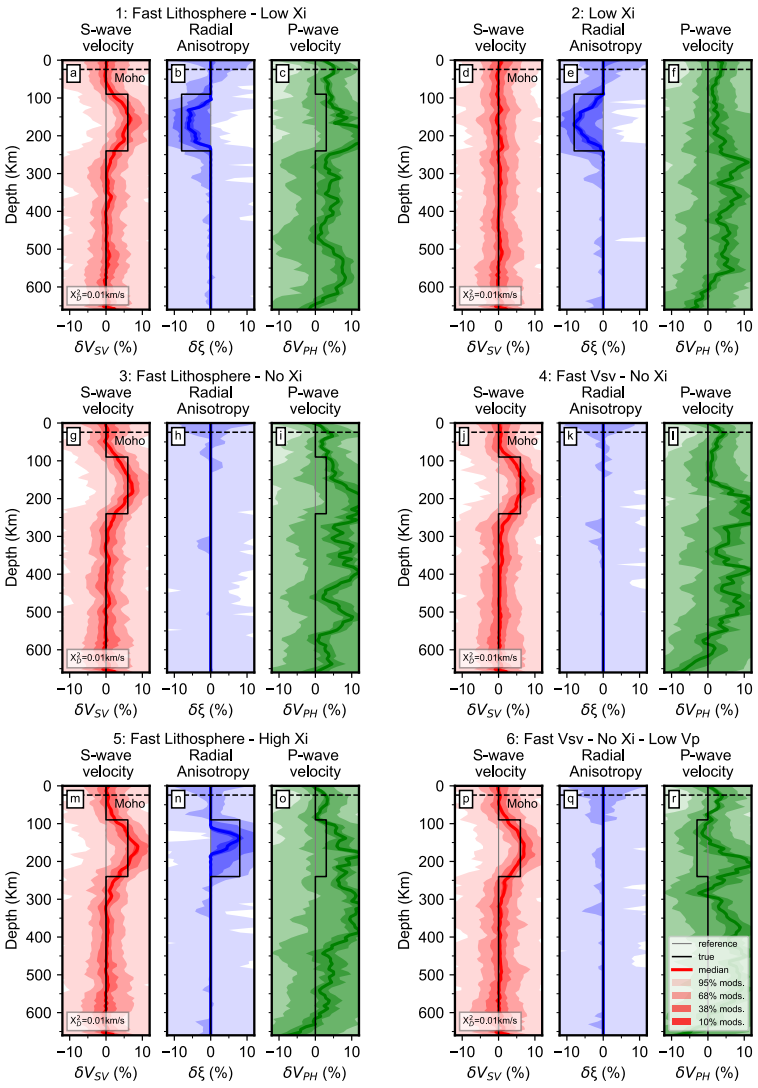

(LEFT) Posterior distributions for VSV (a,d,g,j,m,p), ξ (b,e,h,k,n,q) and VPH (c,f,i,l,o,r) for six synthetic tests with respect to the isotropic reference model (gray line). The preferred median model for VSV (red), ξ (blue) and VPH (green) is shown as a solid, bold line. Confidence intervals (percentage of models) are shown as varying shades of red (VSV), blue (ξ) and green (VPH). The true model (thick black line) and data misfit (XD2) are also shown

(RIGHT) Posterior distributions for VSV (a,d,g,j,m,p), ξ (b,e,h,k,n,q) and VPH (c,f,i,l,o,r) with respect to the isotropic reference model (gray line) for six synthetic test models containing a positive anomaly for both VSV and ξ with increasing vertical extent from 30–180km depth. The preferred median model for VSV (red), ξ (blue) and VPH (green) is shown as a solid, bold line. Confidence intervals (percentage of models) are shown as varying shades of red (VSV), blue (ξ) and green (VPH). The true model (thick black line) and data misfit (XD2) are also shown. Blue circles and orange squares plot depth of maximum negative gradient (transition depth) within ±25km depth of the base of the synthetic anomaly within the VSV and ξ posterior distributions (where possible). ε: depth difference between transition depths and known interface in synthetic model.

Boyce et al., (2024)

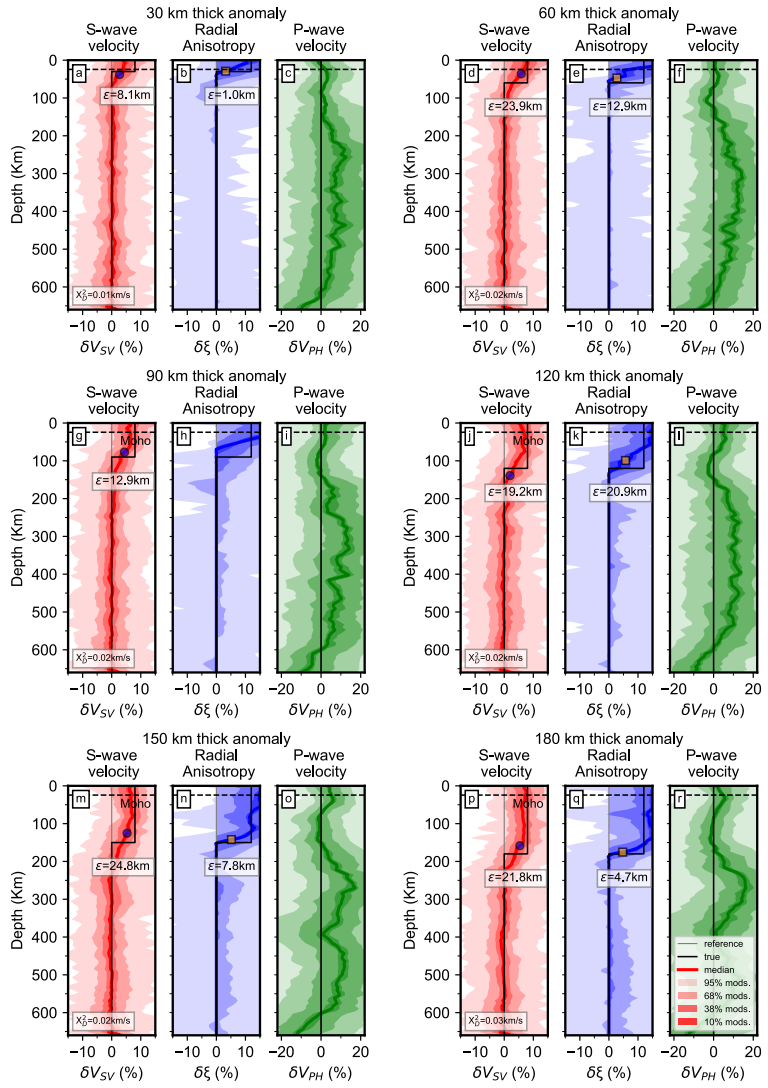

LSQR synthetic tests

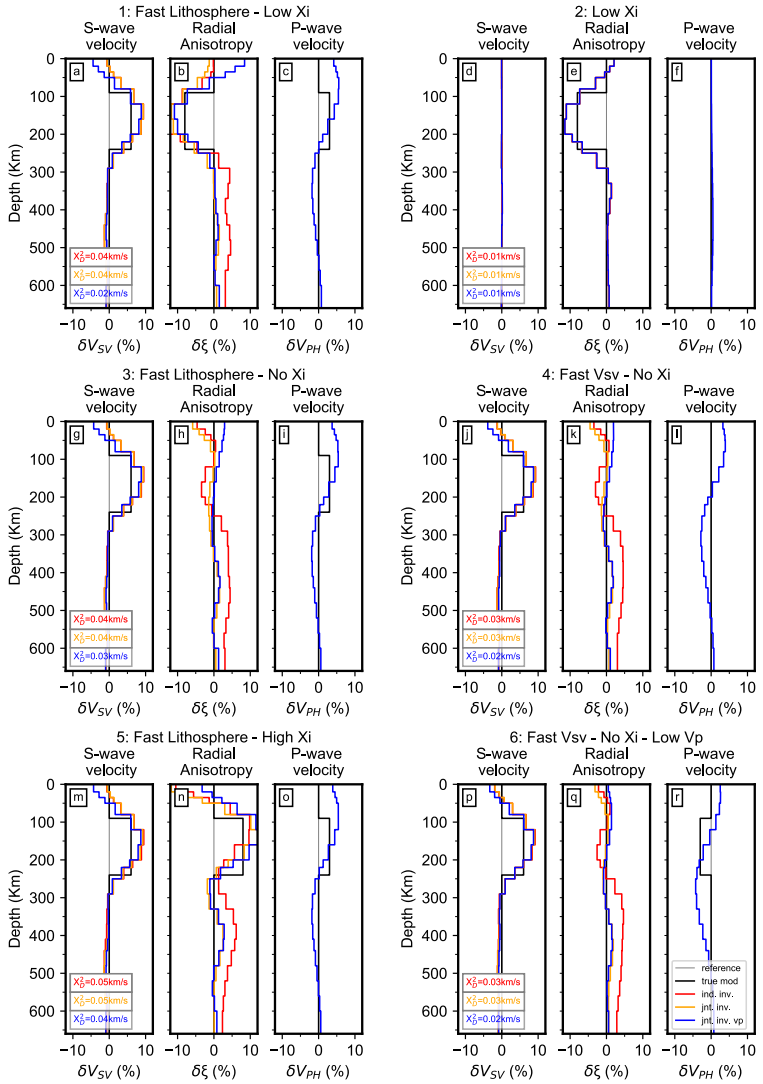

Six synthetic models inverted using variably parameterized LSQR algorithm after Tarantola and Valette (1982); Durand et al. (2015). VSV (a,d,g,j,m,p), ξ (b,e,h,k,n,q) and VPH (c,f,i,l,o,r) shown in percent deviation from the isotropic reference model. Red curve: Independent inversion for VSV and VSH, Orange curve: Joint inversion for VSV and VSH, Blue curve: Joint inversion for VSV, VSH and VPH. The blue curve overlies red and orange curves in cases where inversion outputs are identical. Chi squared data (XD2) fits shown. Reference model (gray line), True model (thick black line).

Boyce et al., (2024)

Bayesian crustal leakage tests

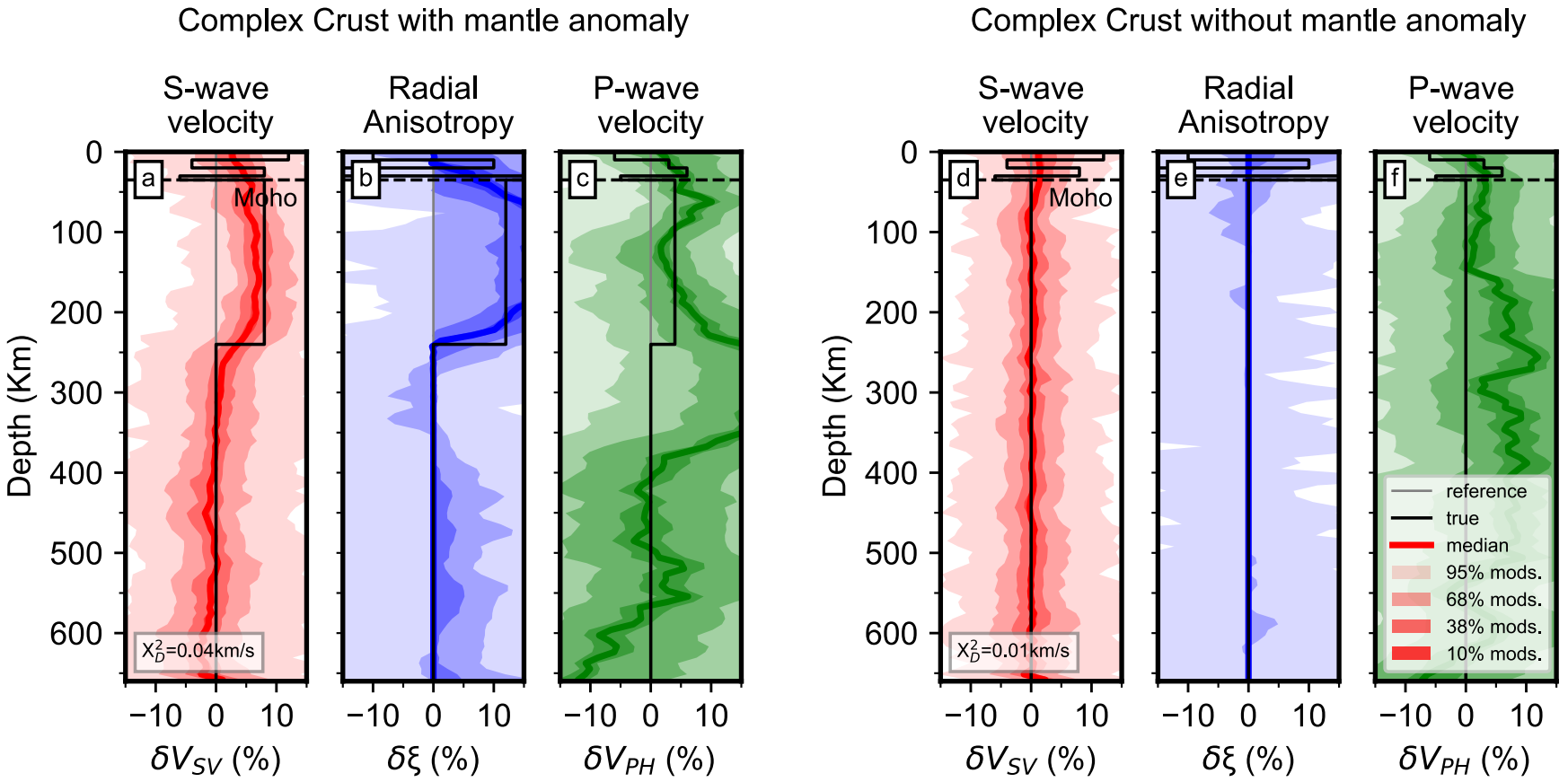

Posterior distributions for VSV (a,d), ξ (b,e) and VPH (c,f) for complex crust synthetic tests with (Left hand side) and without (Right hand side) an underlying mantle anomaly, plotted with respect to the isotropic reference model (gray line). The preferred median model for VSV (red), ξ (blue) and VPH (green) is shown as a solid, bold line. Confidence intervals (percentage of models) are shown as varying shades of red (VSV), blue (ξ) and green (VPH). The true model (thick black line) and data misfit (XD2) are also shown.

Boyce et al., (2024)

Bayesian anisotropic parameterization tests

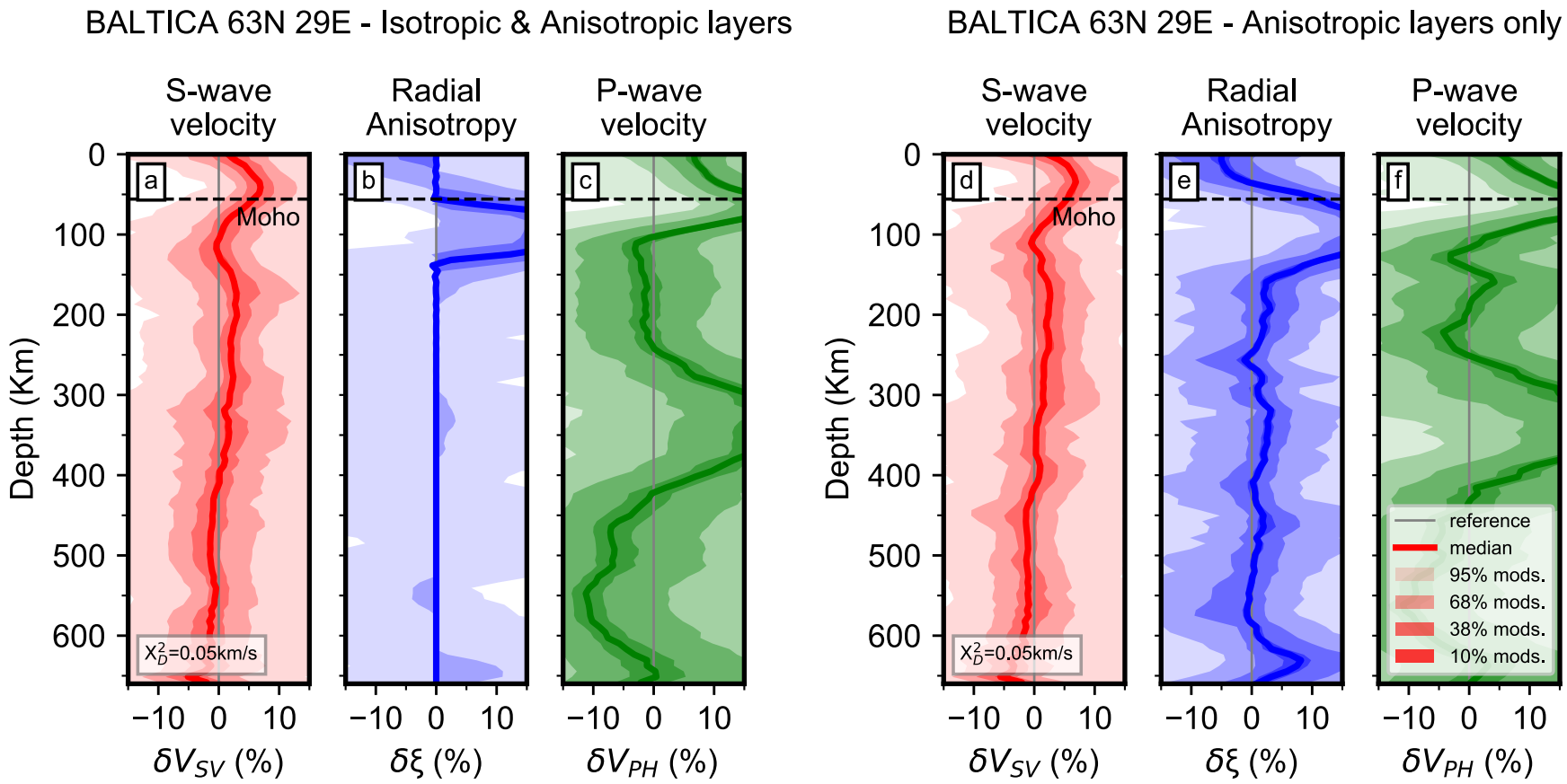

Posterior distributions for VSV (a,d), ξ (b,e) and VPH (c,f) for Bayesian parameterization in which layers can be both isotropic or anisotropic (Left hand side) or all layers are forced to be anisotropic (Right hand side). Models plotted with respect to the isotropic reference model (gray line). The preferred median model for VSV (red), ξ (blue) and VPH (green) is shown as a solid, bold line. Confidence intervals (percentage of models) are shown as varying shades of red (VSV), blue (ξ) and green (VPH). Data misfit (XD2) is also reported.

Boyce et al., (2024)

Bayesian VpH parameterization tests

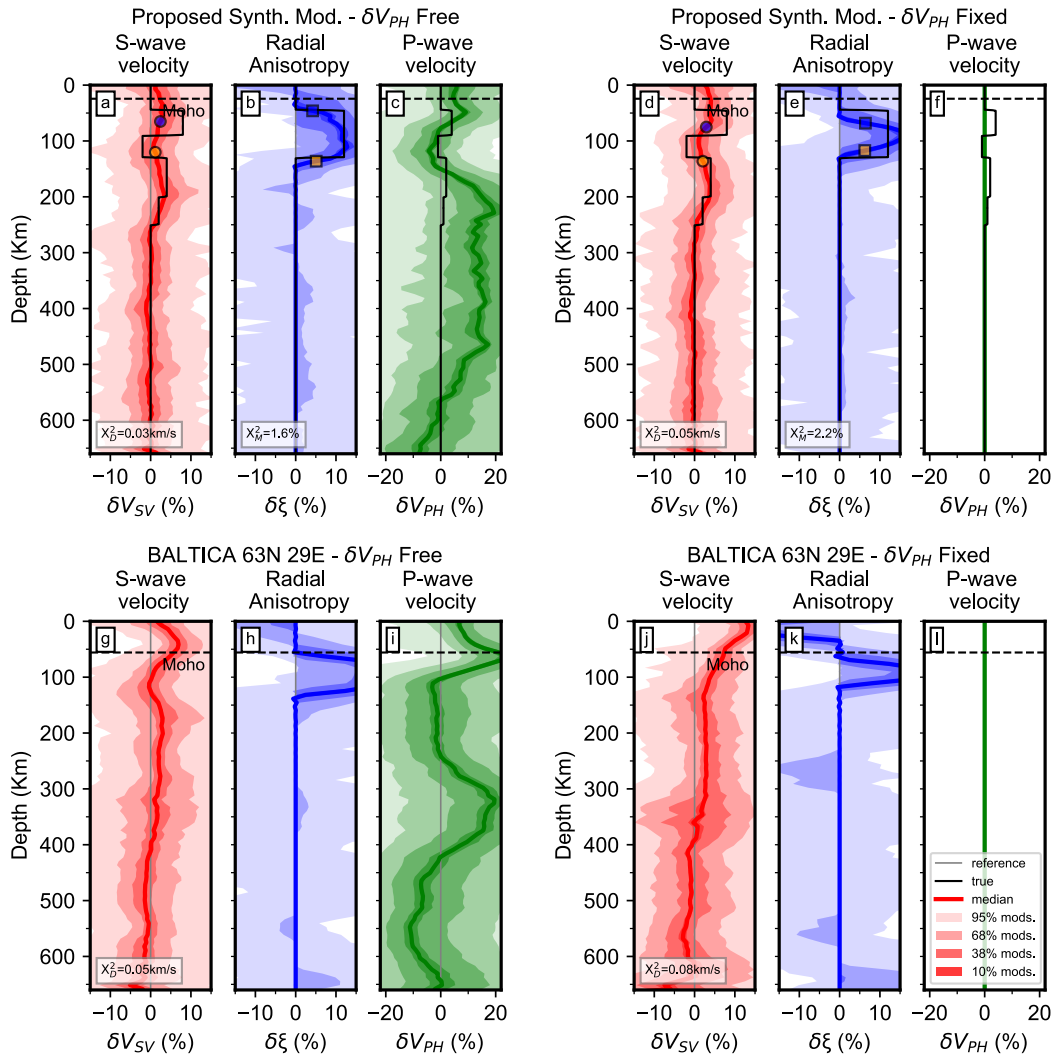

Posterior distributions for VSV (a,d,g,j), ξ (b,e,h,k) and VPH (c,f,i,l) for synthetic model (thick black line, a–f) and real data inversions (g–l). Left hand side shows inversion with VP H - Free parameterization, while the right hand side shows inversion with a VPH-Fixed (to reference model) parameterization. All parameters are plotted with respect to the isotropic reference model (gray line). The preferred median model for VSV (red), ξ (blue) and VPH (green) is shown as a solid, bold line. Confidence intervals (percentage of models) are shown as varying shades of red (VSV), blue (ξ) and green (VPH). Data misfit (XD2) is also reported as well as model fit (XM2) for synthetic tests (a–f). Blue circles and orange squares plot depth of minimum/maximum gradients (transition depths) within ±25km depth of the top and base of low velocity zone (VSV) and positive ξ anomaly within the posterior distributions for synthetic tests (a–f).

Boyce et al., (2024)

Bayesian Craton data inversions

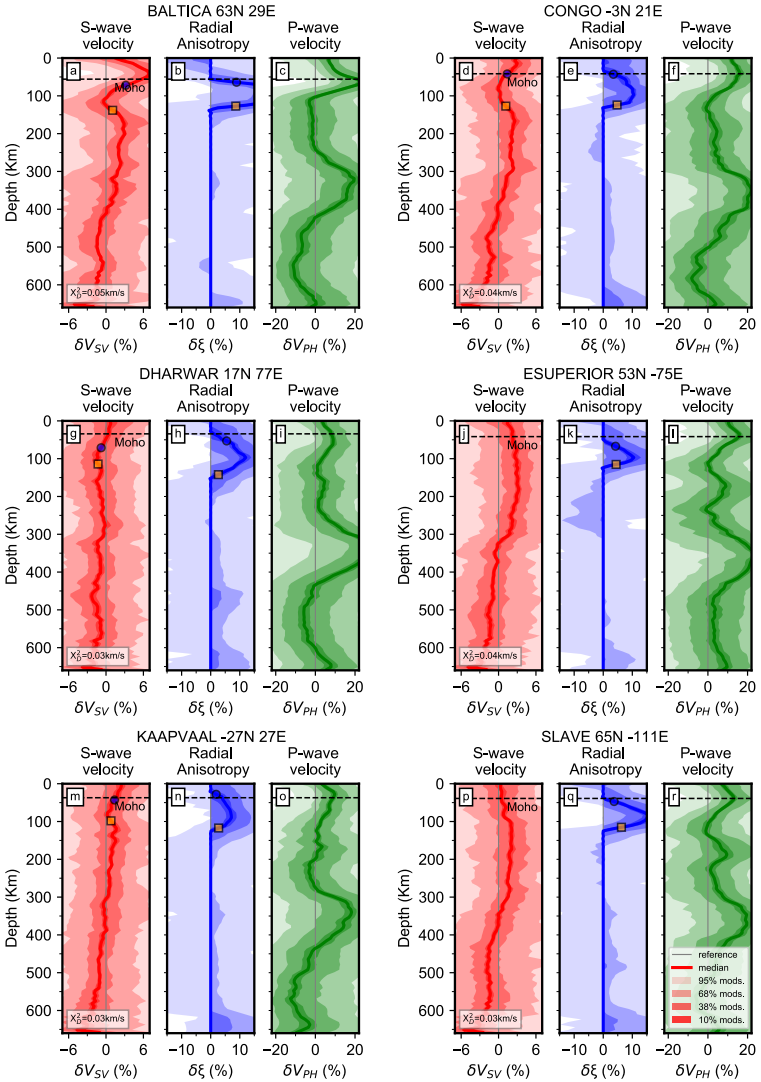

(LEFT) Posterior distributions for VSV (a,d,g,j,m,p), ξ (b,e,h,k,n,q) and VPH (c,f,i,l,o,r) for six cratonic locations (Figure S6) with respect to the isotropic reference model smoothed into Crust1.0 (gray line). The preferred median model for VSV (red), ξ (blue) and VPH (green) is shown as a solid, bold line. Confidence intervals (percentage of models) are shown as varying shades of red (VSV), blue (ξ) and green (VPH). Transition depths (blue circles, orange squares) used in Figure 2 also shown where appropriate. Data misfit (XD2) is also reported.

(RIGHT) Posterior distributions for VSV (a,d,g,j,m,p), ξ (b,e,h,k,n,q) and VPH (c,f,i,l,o,r) for six cratonic locations (Figure S6) with respect to the isotropic reference model smoothed into Crust1.0 (gray line). The preferred median model for VSV (red), ξ (blue) and VPH (green) is shown as a solid, bold line. Confidence intervals (percentage of models) are shown as varying shades of red (VSV), blue (ξ) and green (VPH). Transition depths (blue circles, orange squares) used in Figure 2 also shown where appropriate. Data misfit (XD2) is also reported.

Boyce et al., (2024)

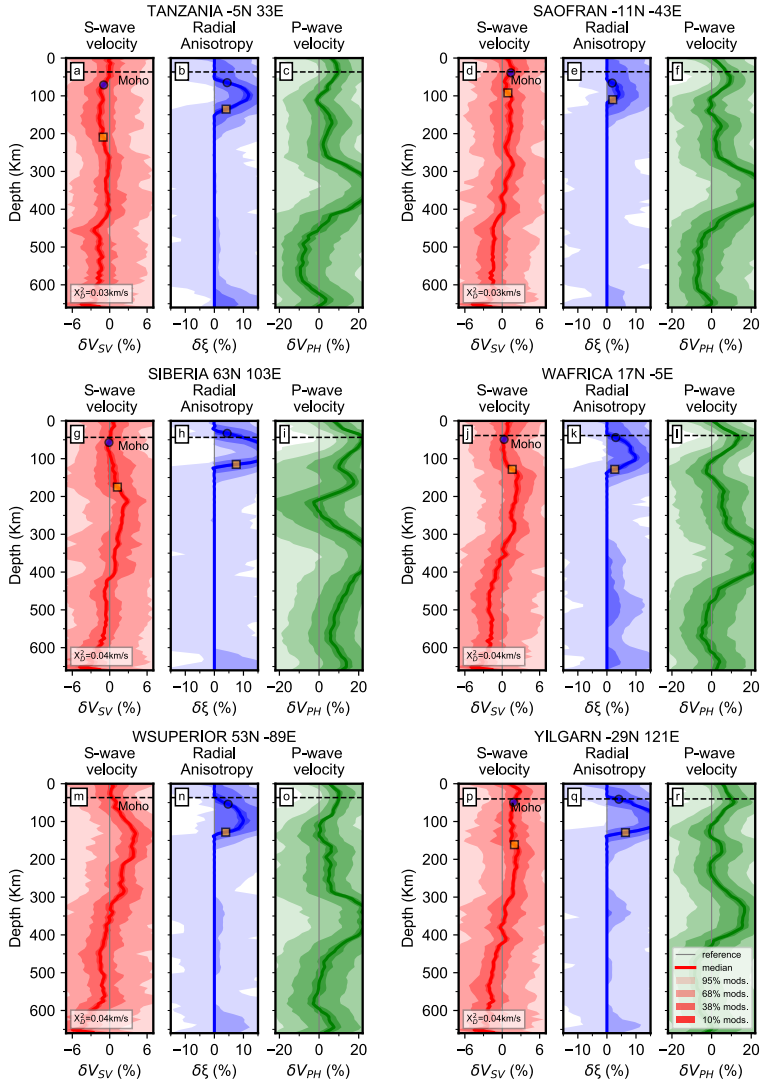

Bayesian Active tectonic and US XC inversions

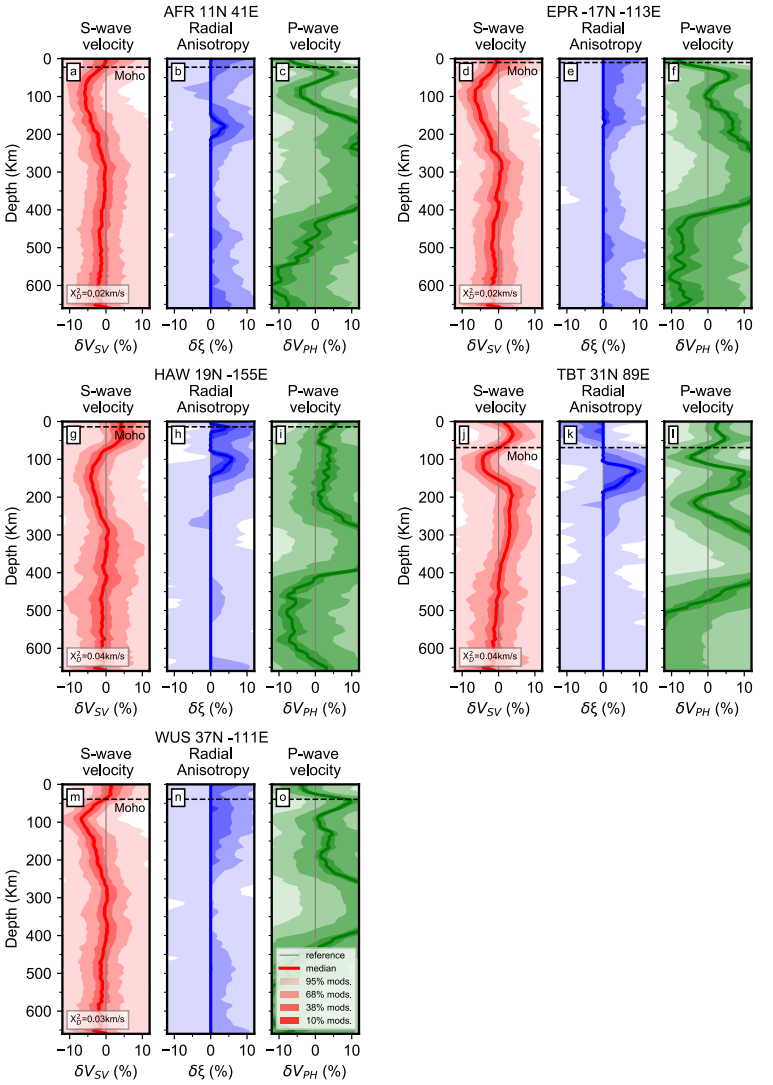

(LEFT) Posterior distributions for VSV (a,d,g,j,m,p), ξ (b,e,h,k,n,q) and VPH (c,f,i,l,o,r) for five active tectonic locations (Figure S7) with respect to an isotropic reference model smoothed into Crust1.0 (gray line). The preferred median model for VSV (red), ξ (blue) and VPH (green) is shown as a solid, bold line. Confidence intervals (percentage of models) are shown as varying shades of red (VSV), blue (ξ) and green (VPH). Data misfit (XD2) is also reported.

(RIGHT) Posterior distributions for VSV (a,d,g,j,m,p), ξ (b,e,h,k,n,q) and VPH (c,f,i,l,o,r) for six cross section points across North America (Figure S8) with respect to an isotropic ref- erence model smoothed into Crust1.0 (gray line). The preferred median model for VSV (red), ξ (blue) and VPH (green) is shown as a solid, bold line. Confidence intervals (percentage of models) are shown as varying shades of red (VSV), blue (ξ) and green (VPH). Data misfit (XD2) is also reported.

Boyce et al., (2024)

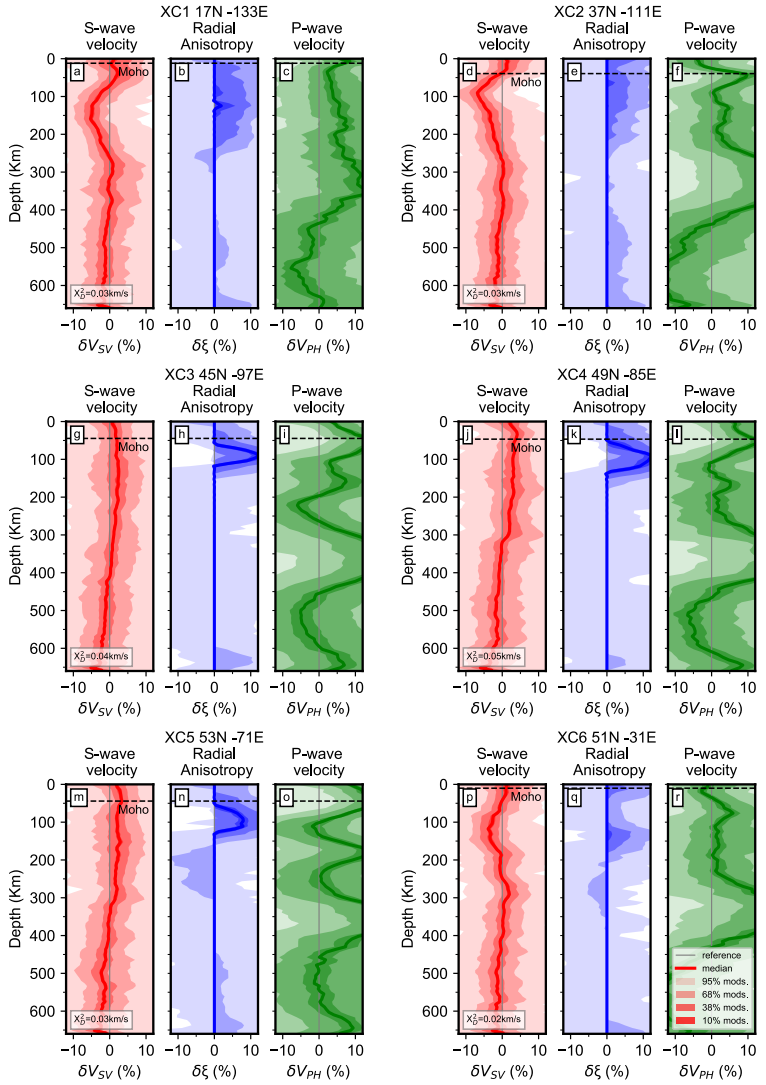

LSQR Craton data inversions

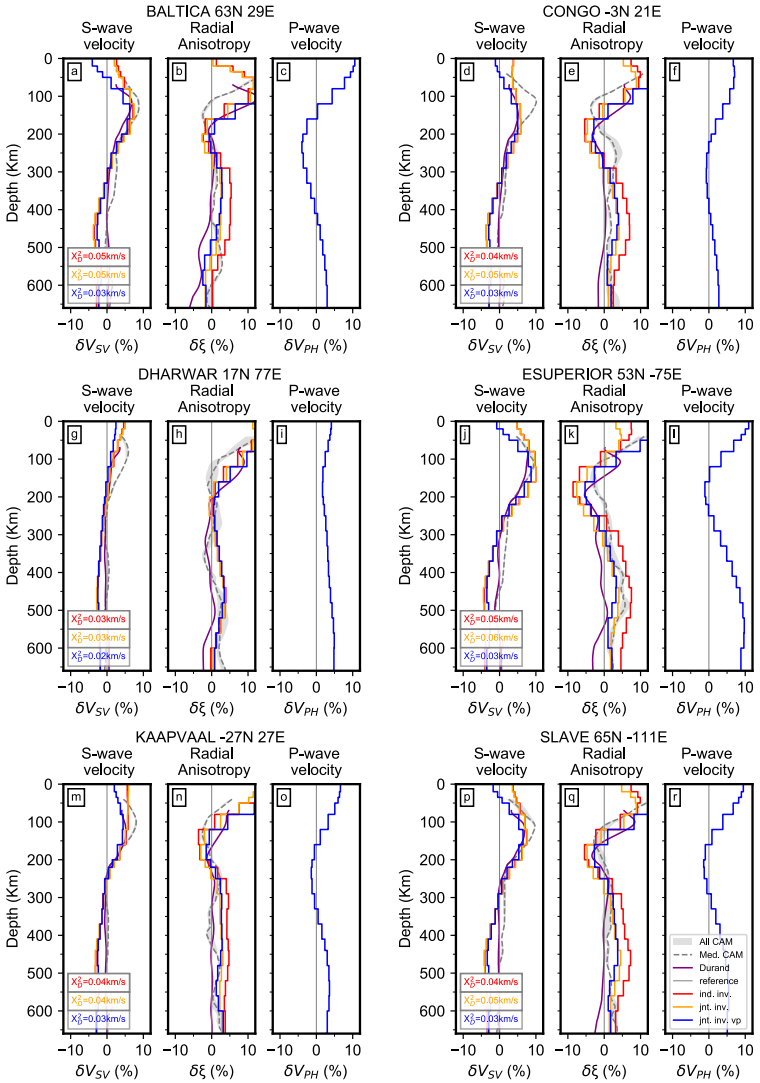

(LEFT) Data from six cratonic locations (Figure S6) inverted using variably parameterized LSQR algorithm after Tarantola and Valette (1982). VSV (a,d,g,j,m,p), ξ (b,e,h,k,n,q) and VPH (c,f,i,l,o,r) shown in percent deviation from isotropic reference model (gray line). Red curve: Independent inversion for VSV and VSH, Orange curve: Joint inversion for VSV and VSH, Blue curve: Joint inversion for VSV, VSH and VPH. Chi squared data (XD2) fits shown. Gray shaded regions and dashed curve (med. mod) show distribution of VSV and ξ profiles from CAM2016 model (Priestley et al., 2020) extracted at each location. Profiles from Durand2023 - unpublished are shown in purple.

(RIGHT) Data from six cratonic locations (Figure S6) inverted using variably parameterized LSQR algorithm after Tarantola and Valette (1982). VSV (a,d,g,j,m,p), ξ (b,e,h,k,n,q) and VP H (c,f,i,l,o,r) shown in percent deviation from isotropic reference model (gray line). Red curve: Independent inversion for VSV and VSH, Orange curve: Joint inversion for VSV and VSH, Blue curve: Joint inversion for VSV , VSH and VPH. Chi squared data (XD2) fits shown. Gray shaded regions and dashed curve (med. mod) show distribution of VSV and ξ profiles from CAM2016 model (Priestley et al., 2020) extracted at each location. Profiles from Durand2023 - unpublished are shown in purple.

Boyce et al., (2024)

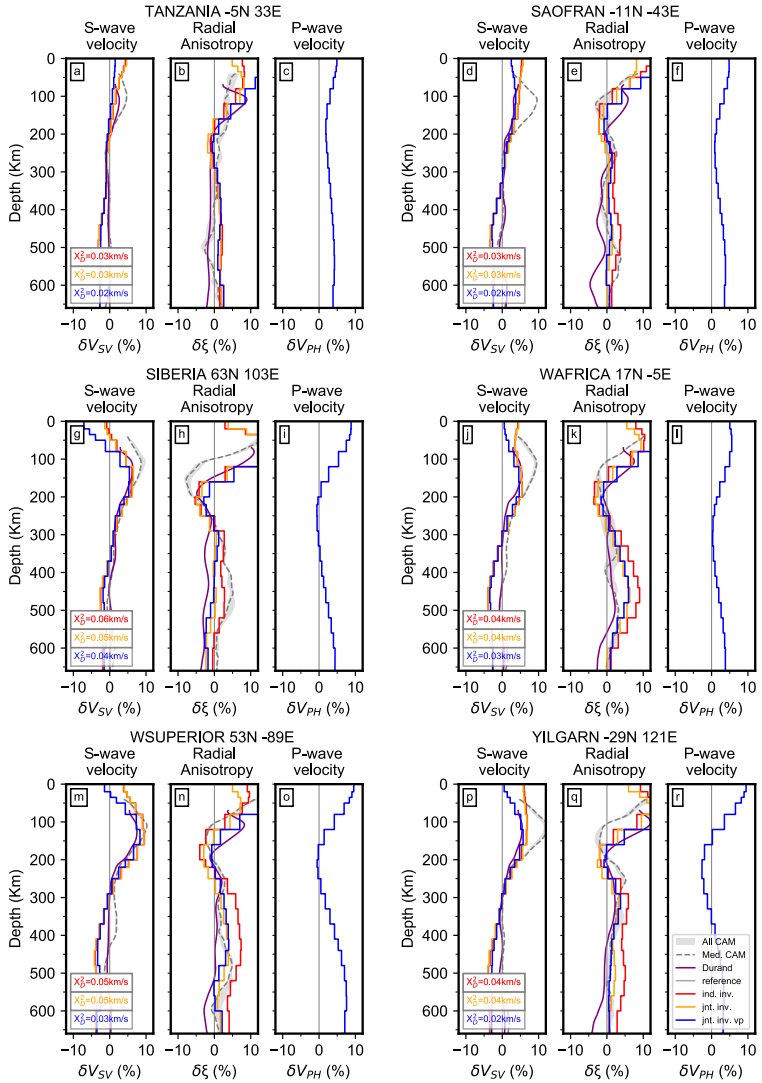

LSQR Active tectonic and US XC inversions

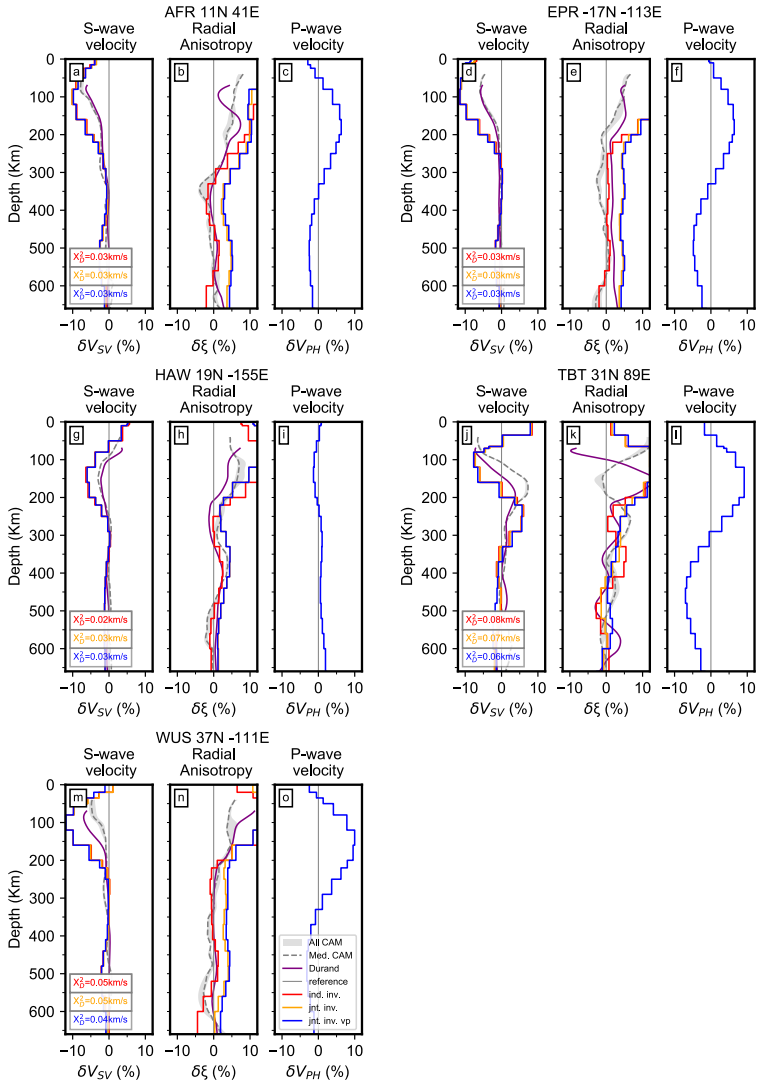

(LEFT) Data from five active tectonic locations (Figure S7) inverted using variably parameterized LSQR algorithm after Tarantola and Valette (1982). VSV (a,d,g,j,m,p), ξ (b,e,h,k,n,q) and VP H (c,f,i,l,o,r) shown in percent deviation from isotropic reference model (gray line). Red curve: Independent inversion for VSV and VSH, Orange curve: Joint inversion for VSV and VSH, Blue curve: Joint inversion for VSV, VSH and VPH. Chi squared data (XD2) fits shown. Gray shaded regions and dashed curve (med. mod) show distribution of VSV and ξ profiles from CAM2016 model (Priestley et al., 2020) extracted at each location. Profiles from Durand2023 - unpublished are shown in purple.

(RIGHT) Data from six cross section points across North America (Figure S8) inverted using variably parameterized LSQR algorithm after Tarantola and Valette (1982). VSV (a,d,g,j,m,p), ξ (b,e,h,k,n,q) and VP H (c,f,i,l,o,r) shown in percent deviation from isotropic reference model (gray line). Red curve: Independent inversion for VSV and VSH, Orange curve: Joint inversion for VSV and VSH, Blue curve: Joint inversion for VSV, VSH and VPH. Chi squared data (XD2) fits shown. Gray shaded regions and dashed curve (med. mod) show distribution of VSV and ξ profiles from CAM2016 model (Priestley et al., 2020) extracted at each location. Profiles from Durand2023 - unpublished are shown in purple.

Boyce et al., (2024)

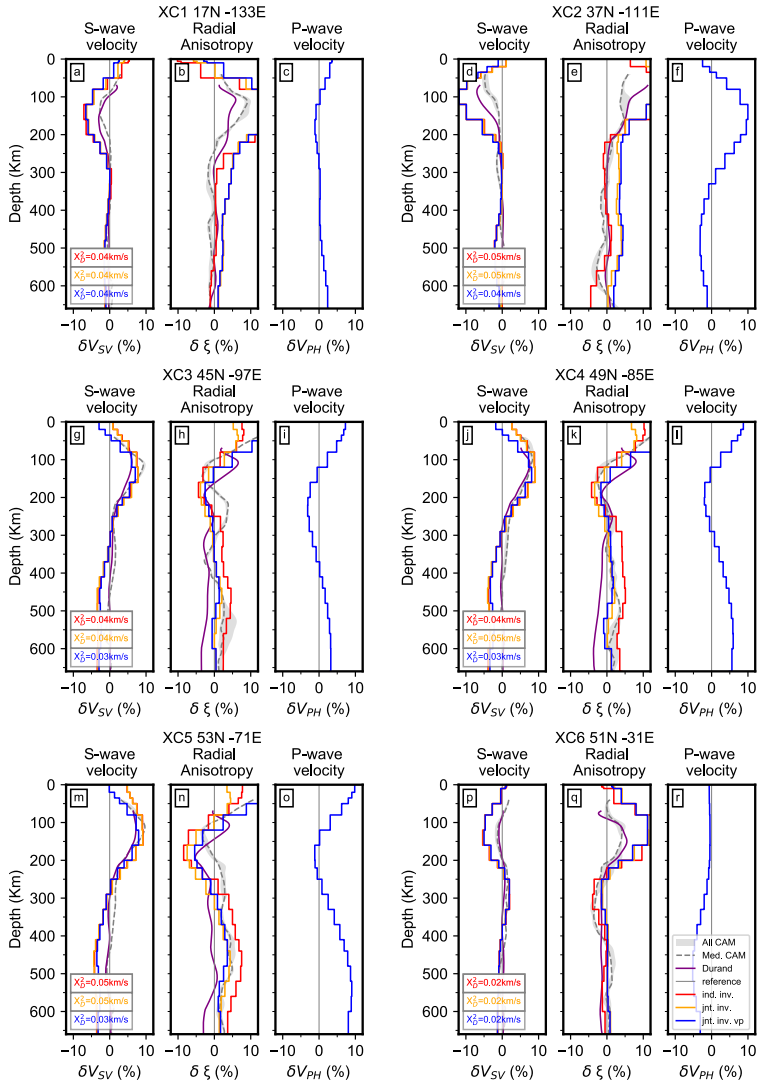

Université Claude Bernard Lyon 1

European Research Council

cnrs

anr agence nationale de la recherche

Bayesian synthetic tests for extrinsic anisotropy

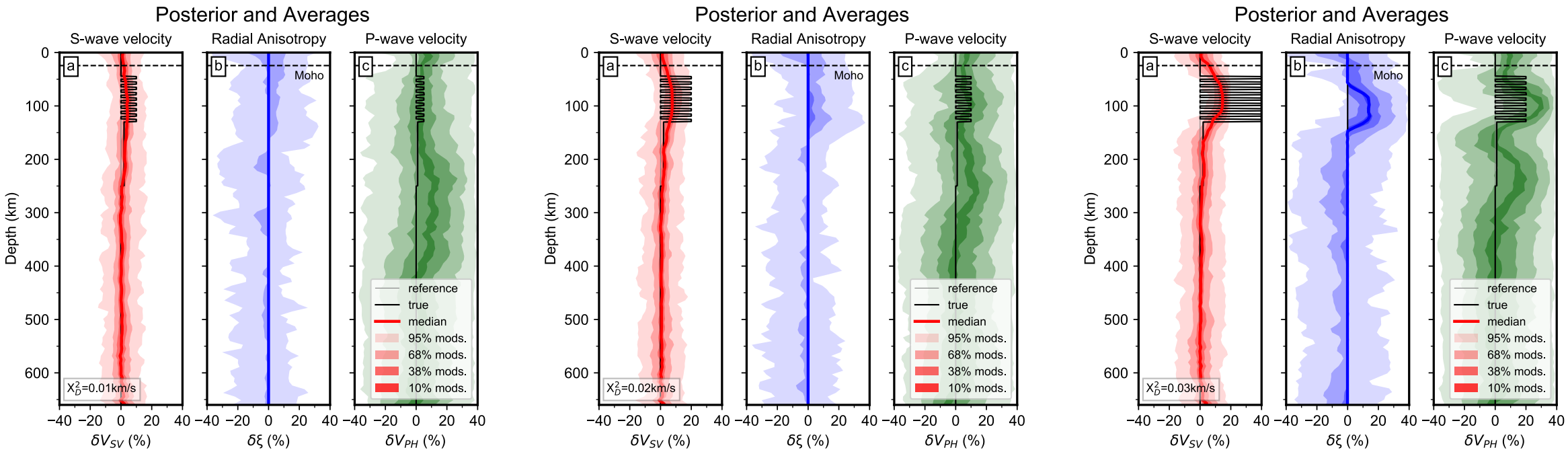

Posterior distributions for VSV (a), ξ (b) and VPH (c) for inversion of an extrinsically anisotropic synthetic model (thick black line, 10% variation – LEFT, 20% CENTER, 40% RIGHT) plotted with respect to an isotropic reference model (gray line). The preferred median model for VSV (red), ξ (blue) and VPH (green) is shown as a solid, bold line. Confidence intervals (percentage of models) are shown as varying shades of red (VSV), blue (ξ) and green (VPH). Data misfit (XD2) is also reported.

Boyce et al., (2024)

Alternate generalized synthetic model

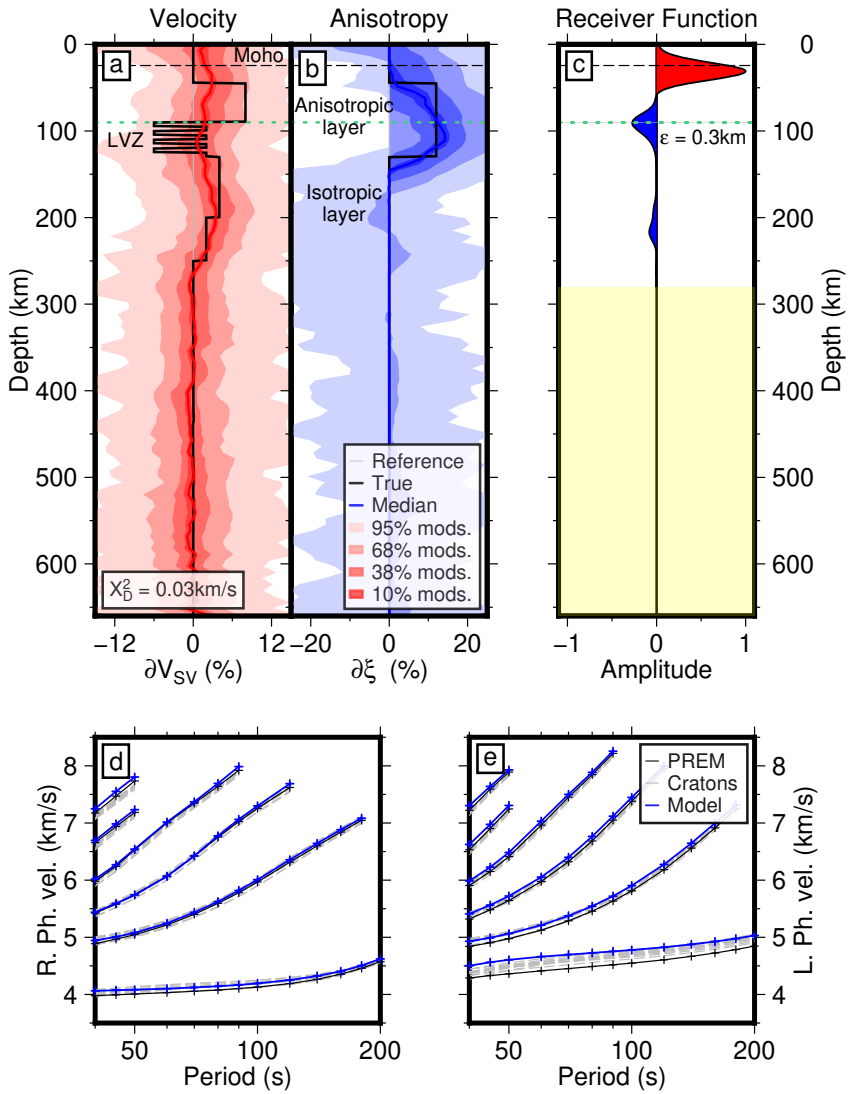

Posterior distributions for VSV (a) and ξ (b) for an alternate generalized synthetic model (bold black line) with respect to the isotropic reference model (gray line). The preferred median model for VSV (red) and ξ (blue) is shown as a solid, bold line. Confidence intervals (percentage of models) are shown as varying shades of red (VSV) and blue (ξ). Data misfit (XD2) is also reported. Axisem simulation (Nissen-Meyer et al., 2014) through synthetic model used to generate S-to-p Receiver Function (RF) stack (c) constructed using RFs between 79-84° epicentral distance. Green horizontal dashed lines show depth difference (ε) between input discontinuity and maximum amplitude on the SRF. Yellow shaded region is below RF stacking depth. Rayleigh (d) and Love (e) fundamental and overtone (1–5) dispersion curves used in the inversions.

Boyce et al., (2024)

Verification of forward modeling

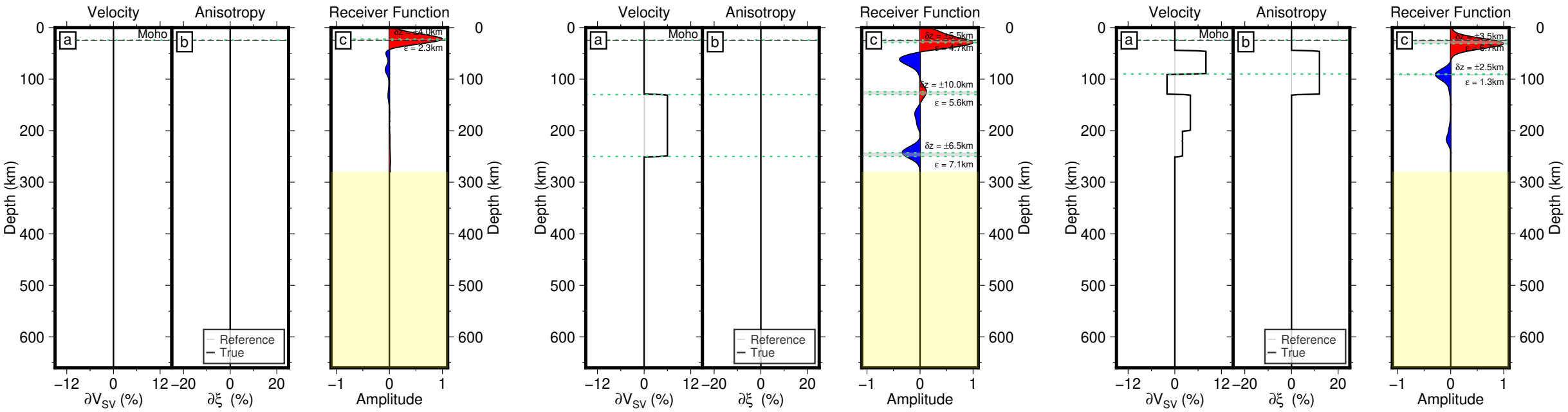

Synthetic δVSV (a) and δξ (b) anomaly models (bold black line) with respect to isotropic reference model (gray line) is used to forward model an S-to-p Receiver Function (SRF) stack (c) obtained from spectral element simulations (Axisem). Green horizontal dashed lines (and gray shaded area between) show depth difference (ε) between input discontinuity and maximum amplitude on the SRF. δz gives the range of depths for each peak within each individual RF trace contributing to the stack.

Boyce et al., (2024)